Dynamical properties of piano soundboards

Antoine Chaigne,[a] Benjamin Cotté, and Roberto Viggiano[b]
Department of Mechanical Engineering (UME), ENSTA ParisTech, Palaiseau, France

(Received 11 May 2012; revised 11 February 2013; accepted 14 February 2013)

In pianos, the transfer of energy from strings to soundboard and the radiation of sound are highly dependent on the dynamical properties of the soundboard. In this paper, a numerical study is conducted for various rib configurations, showing that even slight irregularities in rib spacing can induce a strong localization of the soundboard velocity pattern. The effective vibrating area can be further reduced due to the spatial filtering effect of the bridge. Numerical predictions of modal shapes and operating deflection shapes are confirmed by series of measurements made on upright piano soundboards. Simulations of radiated pressure based on measured and calculated soundboard velocity fields show that localization tends to broaden the cone of directivity and to reduce the number of lobes. © *2013 Acoustical Society of America*. [http://dx.doi.org/10.1121/1.4794387]

PACS number(s): 43.75.Mn [TRM] Pages: 2456–2466

I. INTRODUCTION

As in any stringed instruments, the piano soundboard has a central function. It is coupled to the strings at the "input," and it radiates sound into the air at the "output." The strings are coupled to the soundboard by the bridge which adds noticeable stiffness to it and, in turn, reduces its mobility. The stiffness of the soundboard is also reinforced by ribs glued perpendicular to the direction of the fibers. Usually, the soundboard is slightly curved before stretching of the strings. The static action of the stretched strings then contributes to adding a prestress to the soundboard. As a consequence, it becomes almost flat in normal playing situation. This procedure also helps in maintaining a close contact between string and bridge at the coupling point.[1] The influence of ribs and bridge on the static behavior of the soundboard is well-known and adequately controlled by makers. However, the role played by these components in the dynamical and acoustical properties of the instrument is less understood.

The literature on piano soundboard is rather broad. Bilhuber was one of the first authors to test the influence of some changes in soundboard design on piano tone quality.[2] A pioneering extensive study on soundboard mobility was done by Wogram, who investigated, among other things, the influence of ribs.[3] Using a perturbation method, Müller was able to show the influence of rib properties on the radiation of the lowest modes theoretically.[4] A few years later, Suzuki has shown the link between structural vibrations of the soundboard and radiation. He emphasized, in particular, the efficient radiation of the soundboard above 1.4 kHz.[5] Using a simple model, Giordano has shown the essential influence of ribs on the mechanical impedance of the piano soundboard.[6,7] More recently, Ege and Boutillon have shown that ribs behave as waveguides above nearly 1.1 kHz, and influence the radiation efficiency.[8,9]

The purpose of this paper is to investigate the effects of ribs and bridge on the modal shapes and velocity patterns of the soundboard. As stated by Conklin, the soundboard design on both standard upright and grand pianos is such that the ribs are not perfectly equidistant, although the spacing varies moderately.[10] Such irregularities can have important consequences since even a slight departure from periodic spacing may induce strong spatial localization in some specific frequency range. These phenomena, consecutive to small departure from periodicity in a physical system, were studied originally in solid state physics by Anderson, and are thus often referred to as Anderson's localization.[11] In structural dynamics, a number of cases were investigated by Pierre, who established links between a selected disorder parameter and localization scale.[12,13] Closer to our problem, the localization of modes in irregular rib-stiffened plates was studied by Chen and Xie showing, among other things, that introducing irregularity in rib spacing may result in the reduction of vibration magnitude of some parts of the plate.[14] In piano soundboards, the presence of the bridge further contributes to reducing the vibrating area since, in most cases, it is "viewed" as a rigid obstacle by the modes. These phenomena have an influence on the acoustics of pianos, since the radiation pattern of the soundboard depends on the extension of the spatial velocity field on the soundboard, in terms of magnitude and directivity.

A numerical study is presented in Sec. II, with the objective of investigating the influence of rib spacing and bridge on the vibrations of piano soundboards. This problem is addressed through progressive refinement of the soundboard model. In a first step, modal shapes and frequencies of ribbed plates are calculated up to 5 kHz for three different types of rib spacing: regular (R), slightly irregular (SI), and irregular (I). In a second step, a treble bridge (the large main bridge) is added in order to examine its influence separately. The localization effects are successively examined in terms of modes and operating deflection shapes (ODS). To validate the numerical study, a comparison is made in Sec. III between simulations of a complete soundboard and velocity patterns measured on Pleyel (Paris, France) P131 upright piano soundboards. The ODS are measured on an unstrung soundboard. The rib distribution is slightly irregular. Finally, some consequences of mode localization on soundboard radiation are presented in Sec. IV, in terms of directivity.

[a]Author to whom correspondence should be addressed. Electronic mail: antoine.chaigne@ensta.fr
[b]Present address: 14, Via Tullio Valeri 00041, Albano Laziale Rome, Italy.

II. INFLUENCE OF RIB SPACING AND BRIDGE: A NUMERICAL STUDY

Piano soundboards are complex structures made of the assembly of several components. The most important are the board itself, the ribs, and the bridges. The objective of this paper is to focus on some dynamical properties of ribs and main (treble) bridge. For this purpose, the study starts in this section with a numerical approach where the initial board is progressively complexified through successive addition of ribs and bridge. Attention is paid to the localization of modes due to the irregularity of rib spacing.

A. Presentation of the numerical model

A finite element method (FEM) is developed with the help of the CAST3M software package to study the vibrations of soundboards in terms of eigenfrequencies and modal shapes.[15] A preliminary validation of the finite element (FE) model of ribs and plates is made through comparisons with analytical results based on Timoshenko and Reissner-Mindlin theories, respectively. This validation led to calculate the modes with a set of cubic elements made of 20 nodes each (Cu20) in order to minimize the error. A comparison made between an analytical Reissner-Mindlin model and the FE numerical simulation of a plain rectangular aluminum plate (length = 1.41 m, width = 1.01 m, thickness $h = 9$ mm) with 3621 Cu20 elements shows a maximum error of 1.4% between analytical and numerical eigenfrequencies between 0 and 5 kHz (see Fig. 1). As expected, the frequencies predicted by the FE increase slightly with frequency, due to their artificial stiffening effect, but this effect remains moderate in the observed range. The typical number of elements used for the complete soundboard modeling is selected is equal to 10^4 with some small variations depending on the arrangements and number of the ribs, which is expected to yield a reasonable estimation of the nearly 700 modes in this frequency range. The soundboard has one layer in its thickness, while the ribs have three layers, and the treble bridge has four layers (see also Fig. 10). With this set of data, the number of nodes per wavelength is approximately equal to 20 for the highest modes.

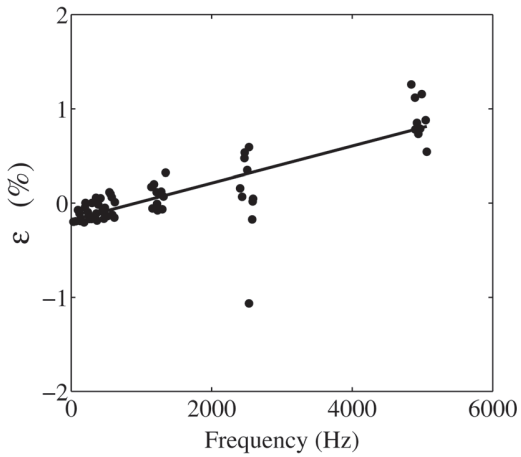

FIG. 1. (•): Numerical error (in %) for the estimation of mode frequencies of a rectangular aluminum plate in four selected bands with the Cu20 FEs, compared to the Reissner-Mindlin theory. (—): General tendency showing the moderate stiffening effect of the elements.

TABLE I. Material parameters used for the ribbed plate and soundboard simulations. *Picea excelsa* (European Spruce) is selected for plate, ribs, and bass bridge. Beech is selected for the treble bridge (see Ref. 17). The density ρ is in kg m^{-3}, the Young's moduli E_L, E_R, and E_T, and the shear moduli G_{LR}, G_{LT}, and G_{RT} are in GPa. The Poisson's coefficients ν_{LR}, ν_{LT}, and ν_{RT} are dimensionless.

Parameters	ρ	E_L	E_R	E_T	G_{LR}	G_{LT}	G_{RT}	ν_{LR}	ν_{LT}	ν_{RT}
Picea excelsa	440	15.9	0.69	0.39	0.62	0.77	0.0036	0.44	0.38	0.47
Beech	674	14	2.28	1.16	1.64	1.08	0.47	0.449	0.518	0.707

The influence of rib distribution on the modes of a clamped rectangular wooden orthotropic plate is investigated first. The area of the plate (1.41 × 1.01 m^2) corresponds to a standard upright piano. The thickness of the plate is 9 mm. Ten ribs of identical and uniform cross-sections (2.1 × 2.5 cm^2) are attached to the plate in a direction perpendicular to the direction of the grain. Material data of *Picea excelsa* Spruce are used for plate and ribs[16] (see Table I). The grain direction forms an angle of 131° with the direction of the longest edge (see Fig. 2).

The lengths of the ribs and the distances between consecutive ribs vary with the type of distribution studied. The different cases of rib spacing are calculated according to the following formula:

$$d_i = d_{\text{ref}}(1 + \alpha_i \beta), \tag{1}$$

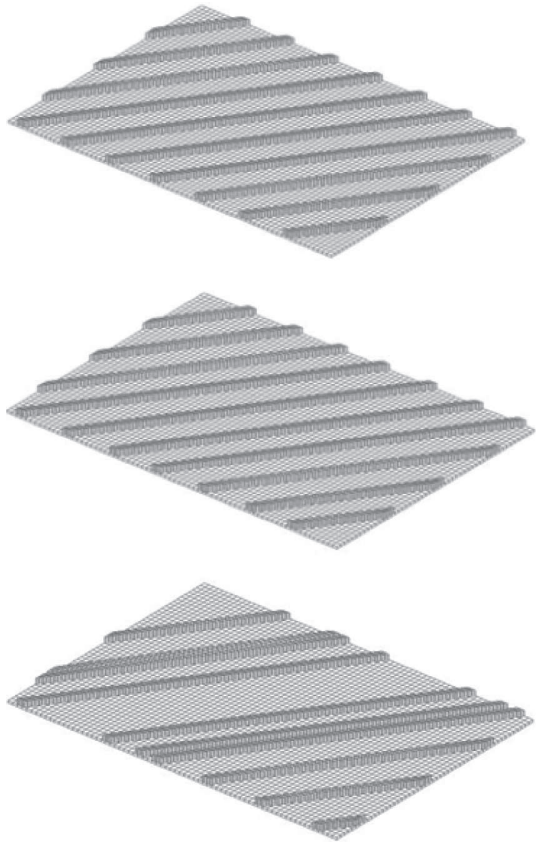

FIG. 2. Plate with various rib configurations. (Top) R, (middle) SI, (bottom) I.

where d_i is the position of the i-rib along the plate, d_{ref} is the distance between consecutive ribs in the periodic configuration, and α_i is a random number with $-1 < \alpha_i < 1$. This series is generated with the *rand* function in MATLAB and yields a uniform distribution. β is a disorder parameter with $0 < \beta < 1$. This simple formula allows to control the irregularity of the rib spacing easily, and yields a better degree of generality to the study than a simple particular case. With $\beta = 0$, the configuration corresponds to a periodic distribution of the ribs. Two irregular cases are reported here (see Table II). With $\beta = 1$ we get a strongly irregular random distribution of rib spacing between 0 and $2d_{\text{ref}}$. This unrealistic spacing is intentionally selected as a limiting case, far beyond the currently observed rib spacing on real soundboards.

For intermediate values of β, configurations are obtained with increasing irregularities as β comes closer to one. Here, a value $\beta = 0.1$ is selected as an intermediate case, which generates a slightly irregular pattern close to those observed on real pianos (see Sec. III). For this SI-case, the mean spacing is 15.64 cm (close to the reference value 15.8 cm, as expected) with a standard deviation $s_d = 0.78$ cm. In terms of $\alpha_i = (d_i - d_{\text{ref}})/(\beta d_{\text{ref}})$ the standard deviation is $s_a = 0.4934$. Recall that the theoretical standard deviation for a uniform distribution $a < \alpha_i < b$ is equal to $(b-a)/\sqrt{12}$,[18] which yields 0.5774 here. The discrepancy between these two values can be attributed to the small number of terms in the series.

Simulations of a ribbed plate with treble bridge are done for the SI rib spacing case. Beech parameters are used for the treble bridge of height 39 mm and width 28 mm. The size and shape of the bridge is similar to the Pleyel P131 upright piano.

B. Results of simulations

1. Influence of rib spacing

As shown in Fig. 3, the distribution of the ribs has only little influence on the lowest modes of the soundboard. A relative difference of 2% on the eigenfrequencies is observed, for example, on the (2,1) mode at 110 Hz between the R and the I rib spacing. Both eigenshapes are comparable. This result is not surprising considering that an equivalent homogenized plate can be defined for any ribbed plate as long as the wavelength is larger than the inter-rib spacing.[19]

The influence of rib spacing becomes visible when the distance between consecutive ribs is comparable to half the structural wavelength.[20] In our example, as observed in usual upright pianos, this corresponds to frequencies higher than 1.0 to 1.2 kHz. Above this frequency limit, the inter-rib spacings can be considered as waveguides.[8,20] Due to their relatively higher stiffness, compared to the plate, the ribs play the role of almost rigid boundary conditions and nodal lines.

TABLE II. Rib spacing configurations for the simulated ribbed plates.

Rib number	1–2	2–3	3–4	4–5	5–6	6–7	7–8	8–9	9–10
R (cm)	15.8	15.8	15.8	15.8	15.8	15.8	15.8	15.8	15.8
I (cm)	17.2	3.5	13.7	30.2	11.3	5.8	17.3	18.6	19.9
SI (cm)	15.9	15.7	14.6	16.4	16.2	14.7	16.0	16.6	14.7

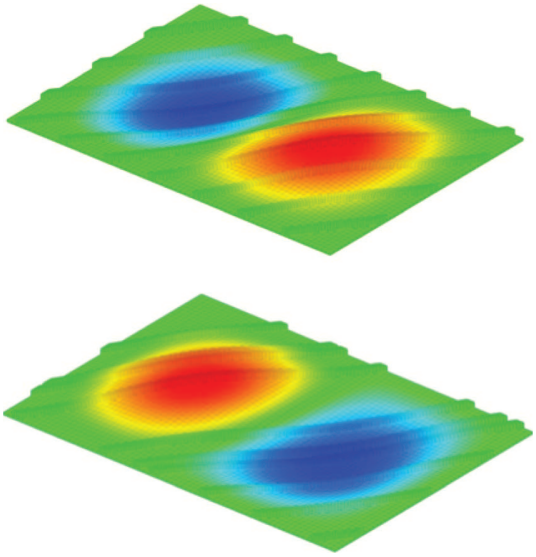

FIG. 3. (Color online) Influence of the ribs on the lowest modes of the plate. (Top) R spacing: $f = 110$ Hz, (bottom) I spacing: $f = 108$ Hz.

As a consequence, the inter-rib distance becomes an important parameter and, in turn, the eigenshapes strongly depend on the rib distribution. To illustrate these phenomena, Fig. 4 shows a comparison between R, SI, and I rib spacing for the same plate, for frequencies near 2 kHz. In the case of periodic (R) spacing of the ribs, the vibration pattern of the soundboard shows that the modes are organized between the ribs, like parallel waveguides, with comparable magnitude in each inter-rib space. In the case of irregular spacing, only two inter-rib zones of the soundboard are vibrating with a significant amplitude. The corresponding mode is said to be localized. The most salient result here is that even a slight departure from R spacing [case (b) in Fig. 4] induces a strong localization of the mode, as predicted by the theory.[12]

2. Influence of bridge and ribs

The model is made progressively closer to a real soundboard through addition of a bridge attached to the ribbed plate on the side opposite the ribs (see Fig. 5). The bridge model is similar in size and location to the treble bridge of an upright piano. A SI pattern [with disorder parameter $\beta = 0.1$ in Eq. (1)] is selected for the ribs. The first consequence is that all eigenfrequencies of the plate increase, due to the stiffening effect of the bridge.

Figure 5 illustrates the reduction of the effective vibrating area consecutive to the presence of the bridge. This follows from the fact that the motion of the bridge is very weak, except at some particular frequencies where it behaves almost like a free-free beam (see measurements in Sec. III). Therefore, for most plate modes, the bridge is viewed as an additional rigid boundary. As a consequence, for slightly irregular rib spacing and for frequencies beyond the "waveguide limit" of nearly 1.1 kHz, the effective vibrating area of the modes is not only localized between a reduced number of ribs, but is often restricted to only one side of the bridge, which can be viewed as a kind of spatial filtering effect. This result is in accordance with the study by Chen

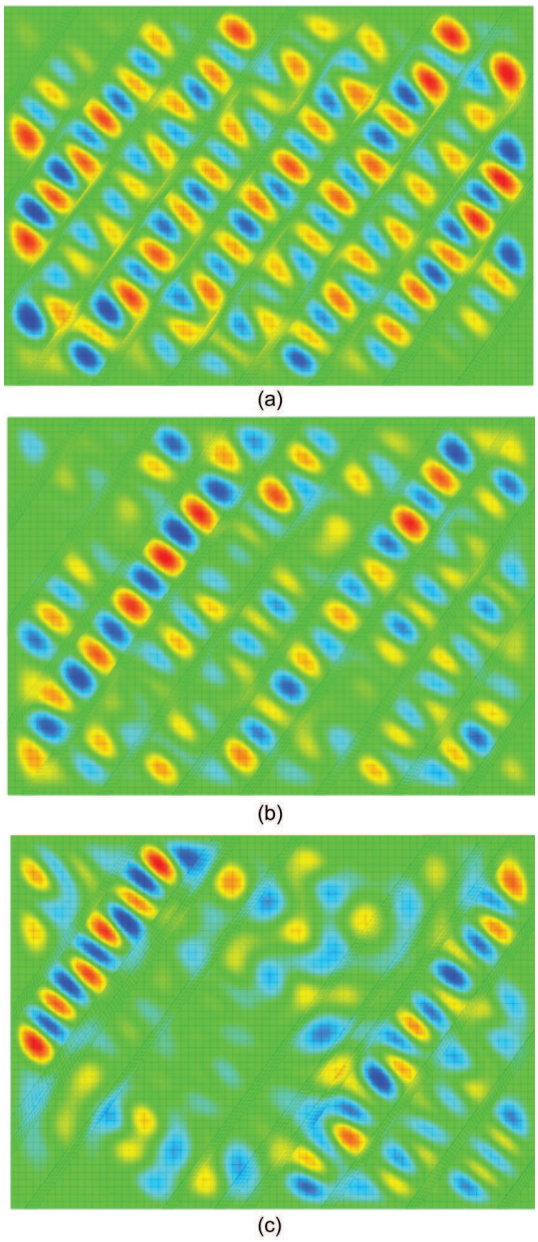

FIG. 4. (Color online) Influence of rib spacing on modes in the medium frequency range ($f > 1.2$ kHz). (Top) R spacing: $f = 2078$ Hz, (middle) SI spacing: $f = 2036$ Hz, (bottom) I spacing: $f = 2075$ Hz.

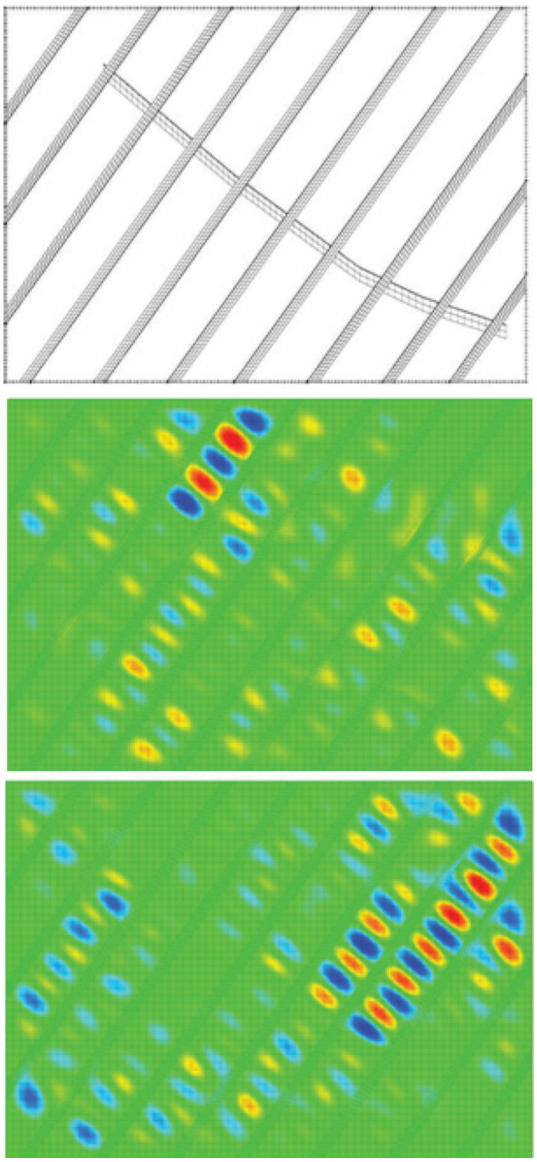

FIG. 5. (Color online) Influence of ribs and bridge on mode localization. SI rib spacing. (Top) Bridge design, (middle) example 1: $f = 2149$ Hz, (bottom) example 2: $f = 2260$ Hz.

and Xie showing that, in presence of a stiffener with high rigidity, the plate behaves as simply supported at the stiffener.[14] As shown later in Sec. IV, this induces significant consequences in terms of radiation and directivity.

From an experimental point of view, it is often difficult to isolate modes of vibrations in the medium and high frequency range because of overlapping. Thus, as shown in Sec. III, what we measure at these frequencies is a harmonic response, or ODS, that can be viewed as the superposition of modal shapes whose eigenfrequencies are close to the excitation frequency. It is thus meaningful to understand the link between modal shapes and ODS, and to check whether mode localization also yields localization of the harmonic response.

From the numerical FE analysis (carried out with the CAST3M software package), we get the modal shape, Φ_n, the modal mass, m_n, and the angular eigenfrequency, ω_n, for the nth mode of the soundboard. A modal loss factor, $\eta_n = 1.5\%$, is chosen. This value is determined by trial-and-error procedure so that satisfactory agreement is obtained between measured and calculated mobilities at the bridge. This order of magnitude is also in agreement with previous studies.[21] The response at some point of coordinates (x_1, y_1) to a harmonic point forcing $F_0 e^{j\omega t}$ at (x_0, y_0) is calculated using the equation

$$\xi(x_1, y_1, \omega) = F_0 \sum_{n=1}^{\infty} \Phi_n(x_1, y_1)\Phi_n(x_0, y_0) H_n(\omega) = F_0 \sum_{n=1}^{\infty} \frac{\Phi_n(x_1, y_1)\Phi_n(x_0, y_0)}{m_n(\omega_n^2 - \omega^2 + j\eta_n\omega_n\omega)}, \quad (2)$$

where $\xi(x_1, y_1, \omega)$ is the displacement of the soundboard in the Fourier domain, and $H_n(\omega)$ is the transfer function of the system for the nth mode. We will now calculate the harmonic response at 2149 Hz, the eigenfrequency of mode

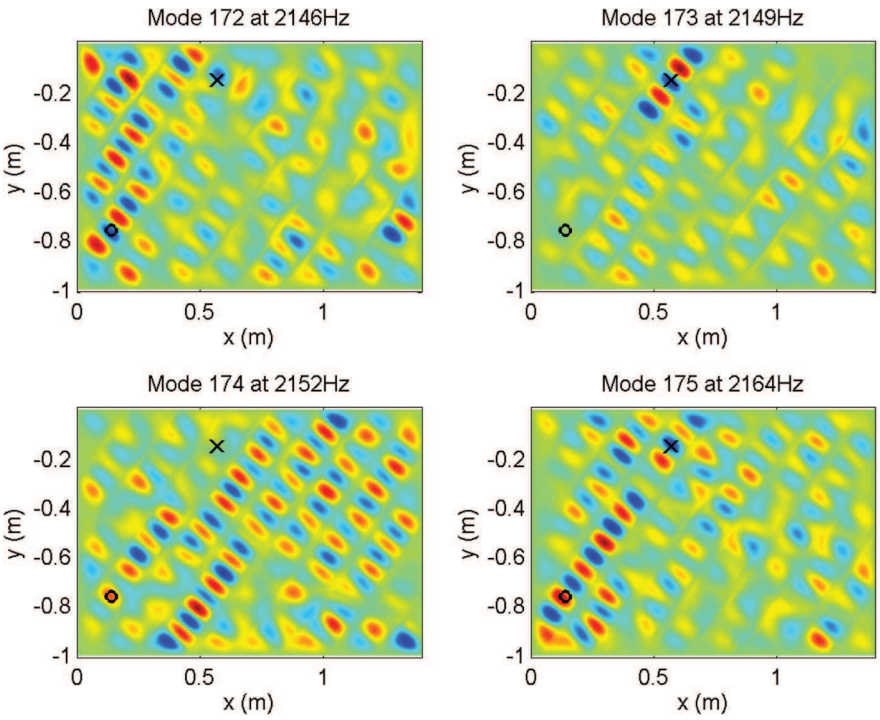

FIG. 6. (Color online) Modal shapes of modes 172 to 175 calculated for the soundboard with SI rib spacing. The excitation point on the upper side of the soundboard is plotted with a cross (×) and the one on the lower side with a circle (○).

173, considering two different excitation points on either side of the bridge. The position of these excitation points is shown in Fig. 6 on the modal shapes of modes 172 to 175. In practice, only a finite number of modes is considered in the summation of Eq. (2). From our experience in the present case, 31 modes are sufficient to obtain the ODS with good accuracy.

To estimate the relative weight of each mode in the total harmonic response, the quantity $|\Phi_n(x_0, y_0)H_n(\omega)|$ is plotted in Fig. 7 for modes 158 to 188 and for both excitation points. For the excitation point on the upper side of the soundboard, at $(x, y) = (57\text{ cm}, -16\text{ cm})$, the mode 173 is strongly excited, as shown in Fig. 6, and the ODS will be dominated by this modal spatial pattern. On the other hand, for the excitation point on the other side of the soundboard, at $(x, y) = (14\text{ cm}, -77\text{ cm})$, mode 173 is weakly excited and modes 172, 174, and 175 will have the strongest influence on the ODS.

The absolute value of the ODS normalized by the excitation force at 2149 Hz is plotted in Fig. 8 for the two

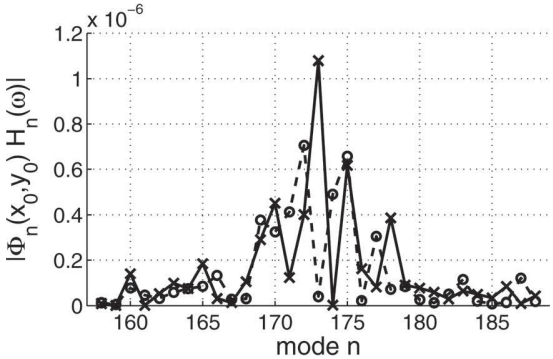

FIG. 7. Weight $|\Phi_n(x_0, y_0)H_n(\omega)|$ of each mode to the total ODS for an excitation point $(x, y) = (57\text{ cm}, -16\text{ cm})$ (×) and an excitation point $(x, y) = (14\text{ cm}, -77\text{ cm})$ (○).

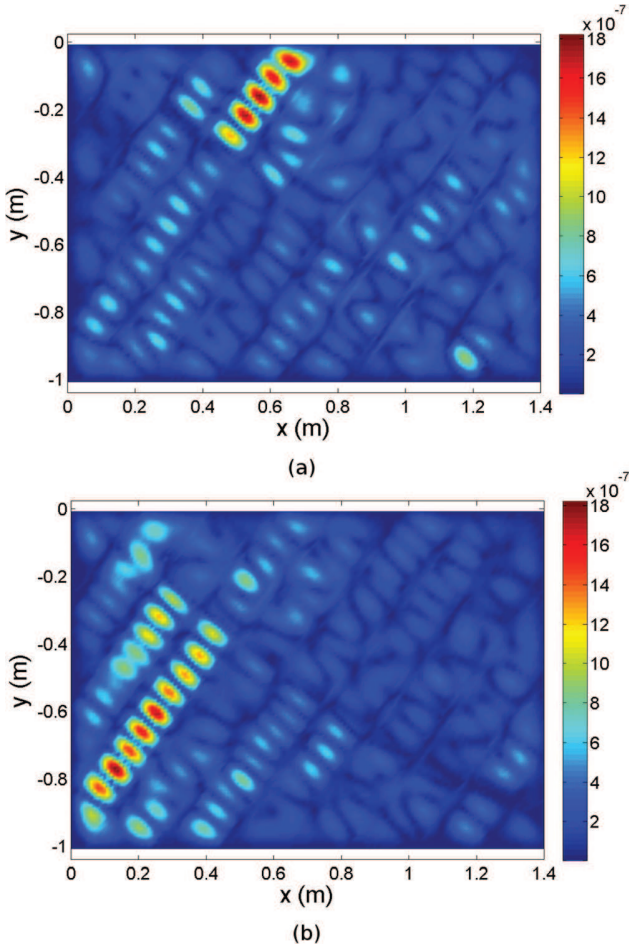

FIG. 8. (Color online) Absolute value of the normalized ODS $|\xi(x_1, y_1, \omega)|/F_0$ at 2149 Hz for (a) an excitation point at $(x, y) = (57\text{ cm}, -16\text{ cm})$, and (b) an excitation point at $(x, y) = (14\text{ cm}, -77\text{ cm})$.

FIG. 9. (Color online) Pleyel P131 unstrung soundboard used for measurements of the ODSs. (Left) Bridge side, (right) ribbed side. The braces are removed for better display.

different excitation points. It appears that the vibration remains localized on the side of the bridge where the excitation point lies. It can be concluded that the harmonic response at a given frequency depends on the excitation position, and that the reduction of the effective vibrating area is also seen in the ODS, even though it corresponds to the summation of several modal shapes with different localization patterns. In order to evaluate the required number of modes for computing an ODS, the harmonic response has also been calculated with only 21 modes (modes 163 to 183). The error between both calculations is given by

$$\mathrm{err}(N_{m2}) = \left[\frac{\sum_{i=1}^{N_p} \left(|\xi(N_{m1})| - |\xi(N_{m2})| \right)^2}{\sum_{i=1}^{N_p} |\xi(N_{m1})|^2} \right]^{1/2}, \qquad (3)$$

where N_p is the number of points on the surface of the soundboard, $N_{m1} = 31$ is the number of modes in the reference calculation, and $N_{m2} = 21$. The error $\mathrm{err}(N_{m2})$ is smaller than 10% for both excitation points, which shows that the influence of the modes decreases as the eigenfrequencies are more distant from 2149 Hz. This calculation also shows that estimating the ODS with 31 modes is reasonably accurate in this range. In the example shown in Fig. 8, the ODS is more localized than some of the individual modes shown in Fig. 6. This result can be explained qualitatively with the help of Eq. (2), which shows that the phase shift between neighboring modes depends on the relative values of their modal shapes, masses, and damping factors. As a consequence, the modulus of the term $\xi(x_1, y_1, \omega)$ might either show a reinforcement or a reduction, of the amplitude in some zones of the soundboard. At this stage, a more extensive quantitative study has to be conducted in order to determine the conditions for increased localization of ODS compared to modes.

III. COMPARISON BETWEEN MEASUREMENTS AND SIMULATIONS

In the second part of the study, comparisons are made between simulated modes based on a FE model of a complete soundboard, and velocity measurements performed on a Pleyel P131 upright piano soundboard. The soundboard is unstrung and the braces are removed for better display of the ODS (see Fig. 9). This removal would not have been possible on a strung soundboard without damage because of the strings tension.

A. Specificity of the complete upright piano soundboard model

Compared to the simplified cases presented in the Sec. II, the upright piano soundboard model now has some additional features and refinements, in order to allow comparisons with measurements. First, the vibrating area of the soundboard is slightly reduced (1.365 m × 0.96 m) considering the fact that a portion is glued to the frame. Treble and bass bridges are attached to the soundboard, and a reduction of cross-section is cut in the treble bridge at the position where it crosses the cast-iron frame. The ten ribs perpendicular to the grain direction show a reduction of thickness at both ends. Two additional beams of constant cross-section (2 cm × 3.5 cm) are attached at the corners of the soundboard, parallel to the grain direction (see Fig. 10). A total number of 12 314 Cu20 FEs are used in the simulations. *Picea excelsa* parameters are associated with the two beams, the ribs, the plate, and the bass bridge. Beech parameters are used for the treble bridge with the grain direction along its length.

The measured distances between consecutive ribs are shown in Table III. This rib pattern roughly corresponds to the SI case presented in Sec. II, with a smaller mean spacing ($d_{\mathrm{mean}} = 13.2$ cm) and a comparable standard deviation $s = 0.97$ cm. By analogy with Eq. (1), the measured rib distribution can be described by the formula

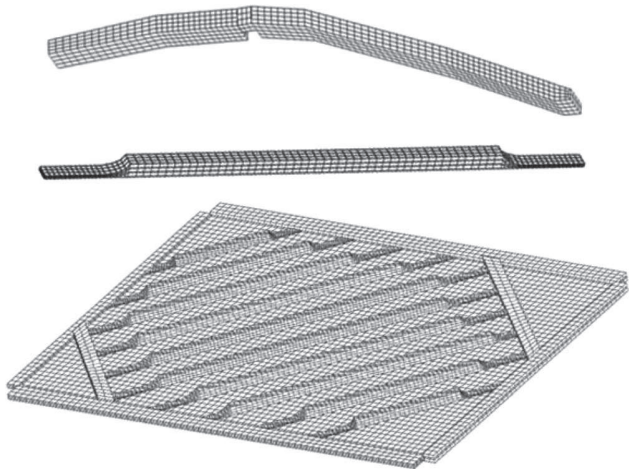

FIG. 10. Complete FE model for the Pleyel P131 upright piano soundboard (ribbed side), rib, and treble bridge.

TABLE III. Measured rib spacing d_i on the Pleyel P131 upright piano soundboards, and α_i values for disorder parameter $\beta = 0.15$.

Rib numbers	1–2	2–3	3–4	4–5	5–6	6–7	7–8	8–9	9–10
d_i (cm)	12.4	13.2	13.4	13.9	14.6	14.4	12.9	12.6	11.6
α_i	−0.496	−0.012	0.109	0.411	0.835	0.714	−0.194	−0.375	−0.98

$$d_i = d_{\text{mean}}(1 + \alpha_i\beta), \tag{4}$$

where d_{ref} is now replaced by d_{mean}. The coefficient $\alpha_i\beta$ lies between -0.1227 and 0.1042 (see Table III). Imposing, as previously, that $-1 < \alpha_i < 1$, yields that the disorder parameter β must be larger than 0.1227. In contrast with the numerical model defined in Sec. III, the experimental series is not an imposed uniform distribution. To illustrate its statistical properties, Fig. 11 shows the α-distribution for $\beta = 0.15$, exhibiting here a reasonable fit with a normal distribution in the range $[-1, 1]$. This difference has no effect on the results. The goal to properly define a disorder parameter is achieved, though the probability to observe d_i close to the limiting values $d_{\text{mean}}(1 \pm \beta)$ is lower in this particular real case than in the arbitrary α-distribution selected in the simulations.

B. Generalities on the experiments

Measurements of soundboard velocity patterns are performed on the unstrung upright piano soundboard whose frame has been removed (see Fig. 9). Removing both strings and frame allows better control of the driving point and larger display of the ODS, however with the drawback that the prestress due to the static tension of the strings is not present. As a consequence, it is anticipated that, as shown by previous authors, the measured eigenfrequencies in the low frequency range (below 300 Hz) will be lower than those observed on a strung soundboard.[22,23] The removal of the frame also has an influence on the boundary conditions.

C. Soundboard motion

1. Low frequencies

In a first series of experiments, the unstrung soundboard is excited with a shaker B&K 4801 (Brüel and Kjaer, Mennecy, France) driven by sweep signals in the range 50 to 500 Hz. The shaker is successively located at two positions: 60 cm from the bottom and 35 cm from the side (between ribs 3 and 4), and 15 cm from the bottom and 11 cm from the side (see Fig. 9). The soundboard is covered with a fine layer of white diffusive painting (Ardrox 9D1B, elmerwallace, Glasgow, UK) on the rib side, and its transverse velocity is measured by a scanning laser vibrometer Polytec (Chatillon, France) PSV300 on a grid of 473 points. Figure 12 shows a comparison between the results of the FE model for some of the lowest modes of the soundboard, and the velocity pattern measured with the laser vibrometer. The measured frequencies correspond to well identified and separated sharp peaks in the velocity spectrum. The measured frequencies and velocity patterns compare well with the calculated eigenmodes and eigenfrequencies. In this frequency range, the deflection shape is not confined between ribs, and the treble bridge does not appear as a nodal line on the velocity pattern.

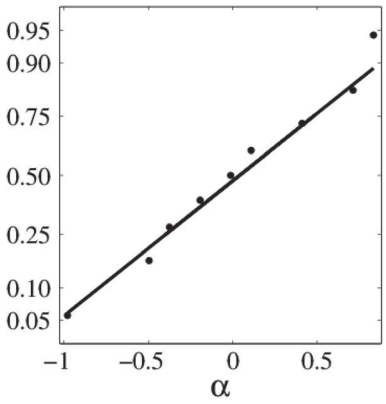

FIG. 11. Comparison between the α-distribution derived from measurements on the Pleyel P131 upright piano (•), and a normal distribution (—).

2. Medium and high frequencies

The measurements grid is refined and contains now 1831 points, in order to study the higher frequencies of the soundboard. Measurements are conducted in the range [1.0,2.5 kHz]. The shaker is still placed at one of the two previously indicated locations, and is driven by bandpass filtered random noise, with variable bandwidth between

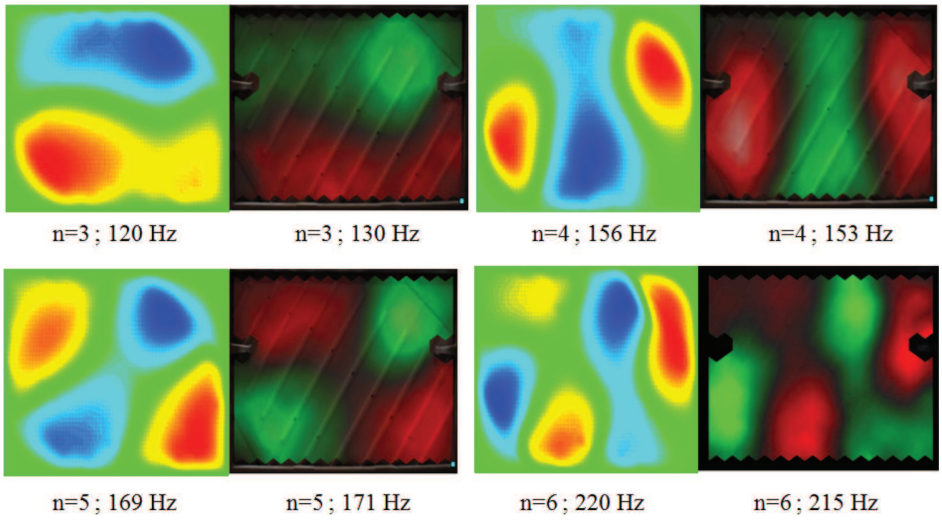

FIG. 12. (Color online) Example of comparison between calculated modal shapes and velocity measurements on the unstrung Pleyel P131 soundboard in the low-frequency range. First and third columns: calculated modes 3 to 6. Second and fourth columns: velocity pattern measurements.

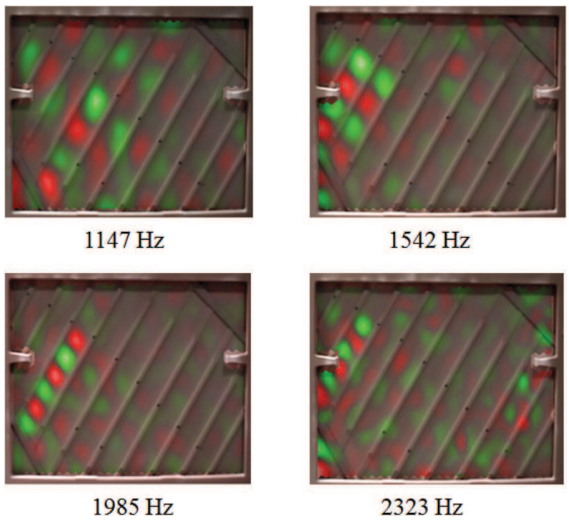

FIG. 13. (Color online) Measured ODS (velocity patterns) at four different harmonic excitations. The exciter is located at the left lower edge of the soundboard (see Fig. 9).

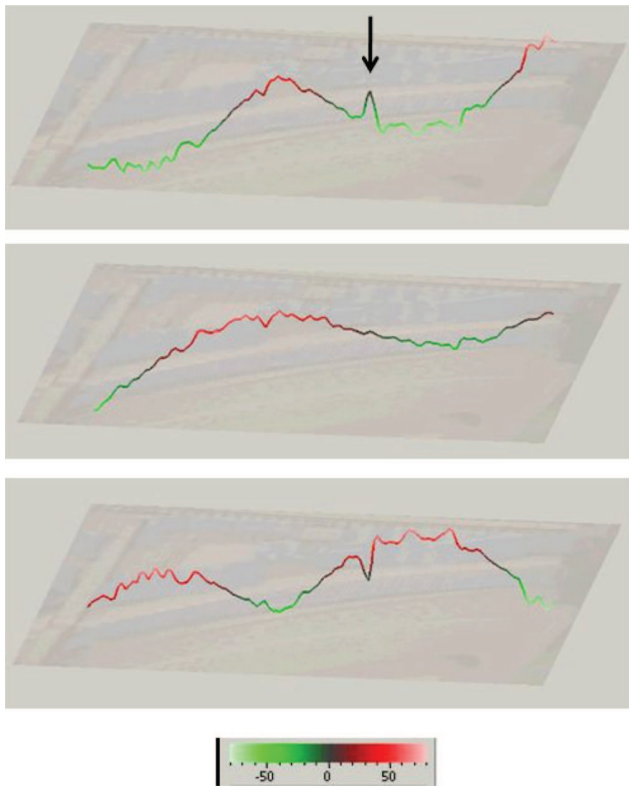

FIG. 14. (Color online) Three successive snapshots showing the motion of the treble bridge at 2010 Hz. The time interval between two successive snapshots is nearly equal to one-fourth of a period. The arrow shows the position of a screw that reduces the motion at this particular point. The unit of the scale is in μm.

100 and 500 Hz. The spectra of the velocity response are averaged over all measurement points. Each spectrum is obtained after averaging over several seconds. The maxima in the magnitude spectrum of the soundboard velocity are detected. The soundboard is then excited at these particular harmonic frequencies. Representative measured velocity patterns are shown in Fig. 13. Because of modal overlapping, low probability exists that each measured shape corresponds to a single mode. It is most likely the combination of several modes, close in frequency. These figures should be compared with Fig. 8, where the calculated ODS were obtaining by summing the contributions of 31 close modes. In most cases, the major part of the vibratory energy remains on the left side of the bridge (the shaker side). In Fig. 7, it was shown that the mode 173 was the main contribution to the ODS shown in Fig. 8 (top), whereas both modes 172 and

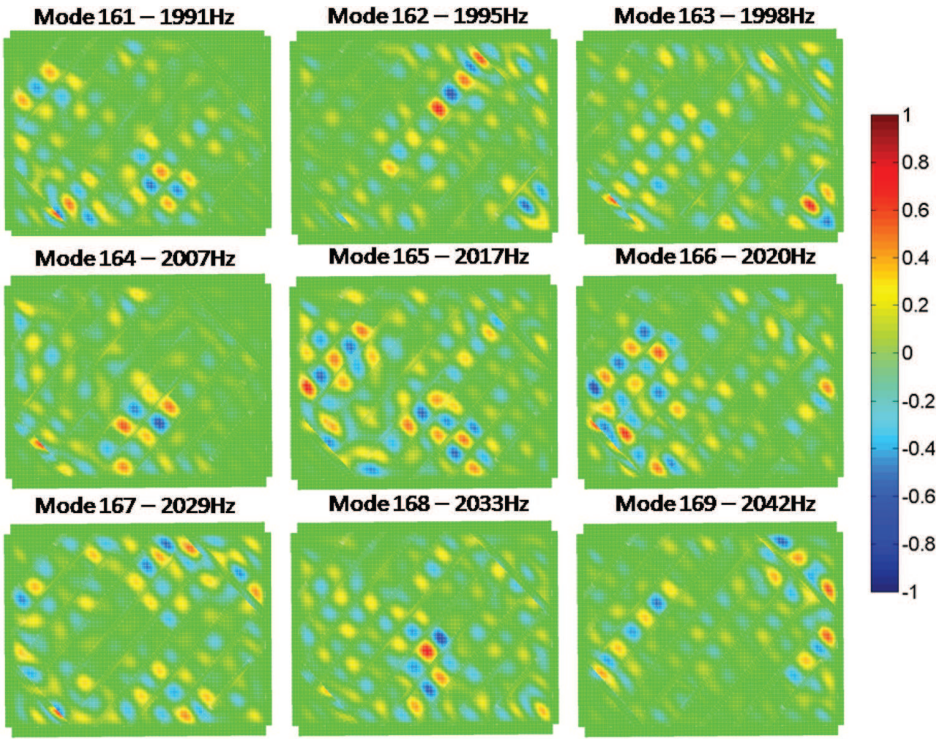

FIG. 15. (Color online) Calculated modes of the complete soundboard close to the bridge mode at 2010 Hz. The amplitude scale is arbitrary.

175 were dominating in the resulting ODS shown in Fig. 8 (bottom). It is likely that similar arguments applied here where only a few localized modes dominate in the observed ODS.

D. Motion of the treble bridge

The motion of the treble bridge, in its upper part (corresponding to the highest notes of the piano), is measured on the strung soundboard by means of the scanning vibrometer in the range 100 Hz to 3 kHz. Below 300 Hz, the bridge acts as a rigid body. For frequencies above 300 Hz, its motion exhibits a few well defined transverse modes comparable to those of free beams. Figure 14 illustrates one example of such motion at 2010 Hz. The observed peak in the displacement shape, situated near the middle of the bridge (see the arrow in Fig. 14), corresponds to the position of a screw that reduces the amplitude of the motion considerably at this point. One direct consequence of bridge motion is that, at these particular eigenfrequencies, the coupling conditions of the strings change dramatically depending on the position of the string end. Except at these few frequencies, the motion of the bridge is significantly smaller than the one of the soundboard, and can be thus regarded as an almost fixed boundary for the soundboard. These experiments shed another light on the previously described filtering effect of the bridge that results in a reduction of the effective vibrating area of the soundboard.

To illustrate this bridge filtering effect further, Fig. 15 shows nine calculated modes of the complete soundboard in the vicinity of the bridge mode at 2010 Hz shown in Fig. 14. The bridge (not seen here) is almost perpendicular to the ribs, as shown in Fig. 5. These results show that for almost all modal shapes the zones with significant amplitude (dark zones in gray scale) are situated mainly on one side of the bridge, except for the mode 165 at 2017 Hz and, to a lesser extent, for the mode 163 at 1998 Hz.

IV. EFFECT OF MODE LOCALIZATION ON SOUNDBOARD RADIATION IN THE MEDIUM RANGE

The purpose of this section is to examine the effects of ribs and bridge on the radiated directivity pattern of a piano soundboard in the far field. A Rayleigh integral is used for calculating the radiated sound pressure, thus the soundboard is supposed to be in baffled conditions. These conditions are not realistic for a piano soundboard in the complete audio range. However, the effect of the baffle is significant for acoustic wavelengths larger than the characteristic dimensions of the source only.[24] Since the frequency domain of interest here is in the range 1 to 3 kHz, the maximum acoustic wavelength in air is 30 cm, which can be considered as reasonably small compared to the dimensions of the soundboard.

The pressure is calculated on a hemisphere at a distance of $r = 3$ m from a reference point on the soundboard, which is compatible with the assumption of far field. Figures 16 and 17 show two distinct representative examples of directivity patterns. In the first case, directivities are obtained from a modal shape calculated with a R rib distribution, while in the second case, they are obtained from a measured harmonic response. The relationship between modal shapes and harmonic response (or ODS) has been studied in Sec. II B. The origin and directions of the X- and Y-axis, in each case, are indicated in the figures. The directivity versus the angle θ (respectively, ψ) shows the angular distribution of the pressure magnitude in the plane perpendicular to the soundboard in the direction of the X-axis (respectively, Y-axis). The X-axis corresponds to the direction of the ribs, while the Y-axis is perpendicular. It has been tested that the choice of the origin of the coordinate system $X - Y$ has a weak influence on the calculated directivities with $r = 3$ m.

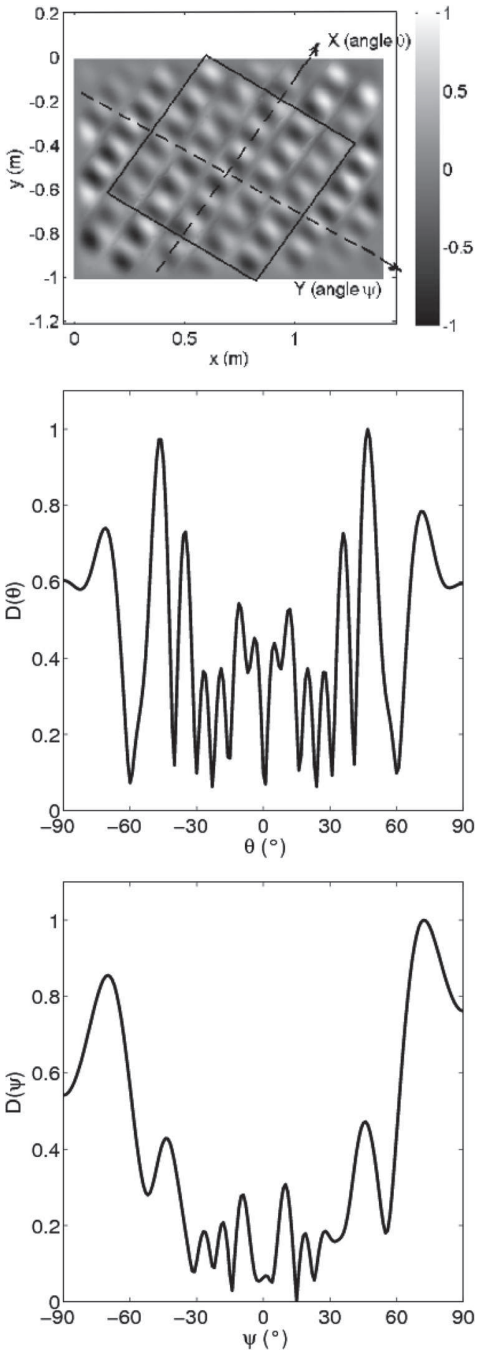

FIG. 16. (a) Displacement field calculated for the ribbed plate with R rib distribution at 2078 Hz, and associated directivities (b) $D(\theta)$ along the X-axis, and (c) $D(\psi)$ along the Y-axis calculated at $r = 3$ m.

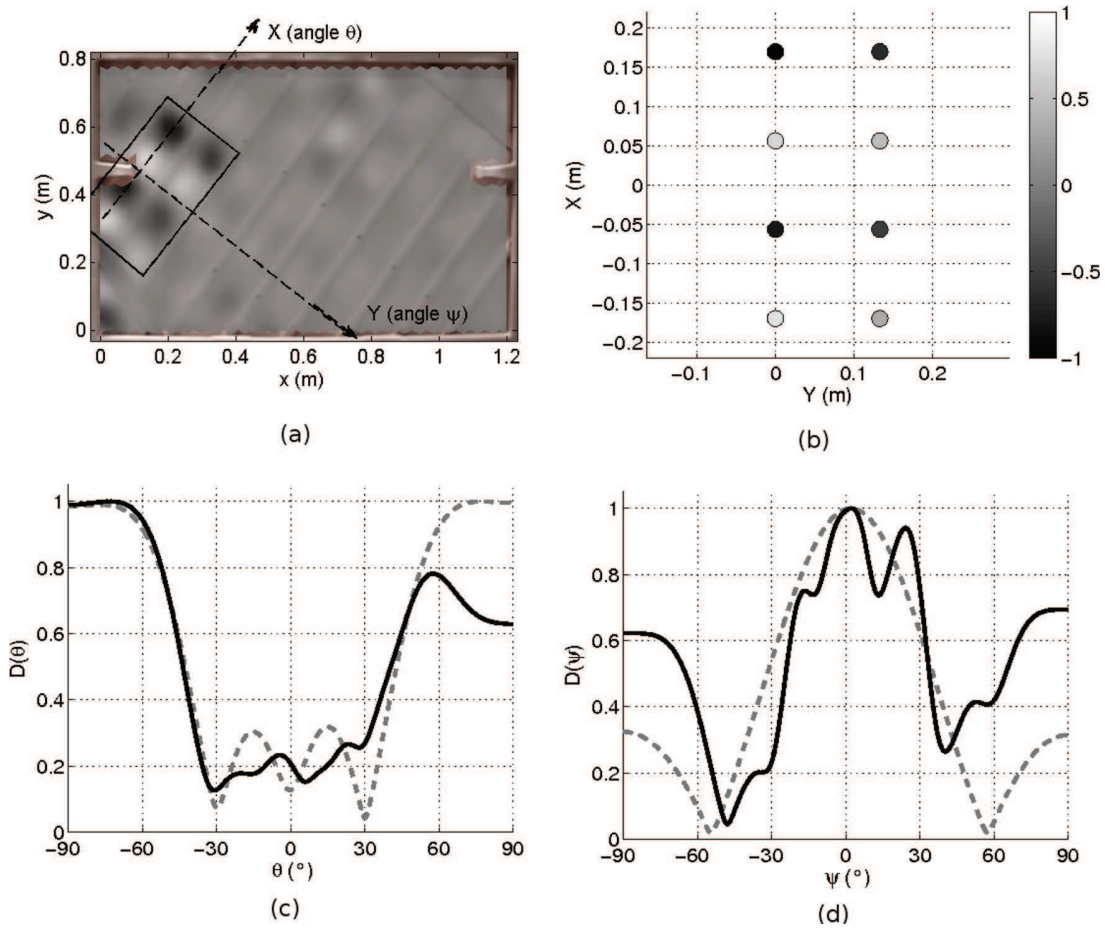

FIG. 17. (Color online) (a) Velocity field measured at 1542 Hz, (b) configuration of a 2-D array of 4 × 2 monopole sources, and corresponding directivities (c) $D(\theta)$ along the X-axis, and (d) $D(\psi)$ along the Y-axis. The directivities are calculated at $r = 3$ m for the measured velocity field (—) and for the 2-D-array (- - -).

In Fig. 16, the modal directivity is calculated for a ribbed plate with R rib distribution defined in Sec. II, without a bridge, and vibrating at a frequency of 2078 Hz (mode 160). At this mode, the entire plate is vibrating like a two-dimensional (2-D) array of elementary sources, with nodal lines along the X-axis merged to the ribs. Both directivity patterns [$D(\theta)$ along X, and $D(\psi)$ along Y] show a relatively high number of lobes, as it is commonly observed for such arrays.

Figure 17 shows a different situation. The pressure directivity here is calculated from the velocity field measured on the unstrung soundboard at frequency $f = 1542$ Hz. The shaker is located 15 cm from the bottom and 11 cm from the side (see Fig. 9). At this frequency, both the bridge and the SI rib distribution contribute to reduce the effective vibrating area of the soundboard. The consequences of this localization can be seen on both directivity patterns $D(\theta)$ and $D(\psi)$, where the number of lobes is strongly reduced compared to the previous case. Also the angular selectivity of the lobes is less sharp.

To check the consistency of these results, the directivities calculated from the measured velocity field are compared to the directivities of a 2-D array of 4 × 2 monopole sources whose amplitudes correspond to the eight extrema of the boxed region in Fig. 17(a). The distance between monopole sources is 11.3 cm along the X-axis and 13.3 cm along the Y-axis, as can be seen in Fig. 17(b). The directivities along X and Y are in relatively good agreement for both calculations, which shows that the reduced vibrating area delimited in the boxed region of Fig. 17(a) is responsible for the directivity patterns plotted in Figs. 17(c) and 17(d).

V. CONCLUSION

The results of a numerical FEM study show that small irregularities in the spacing of the ribs can have strong localization effects in soundboards, both on modes and on ODS. In addition, both numerical modeling and experiments show that the presence of the bridge further contributes to reduce the size of the vibrating area. This is due to the fact that, except for a few particular frequencies, the bridge acts as a rigid obstacle for the waves propagating on the soundboard. Localization effects are visible for frequencies above 1.0 to 1.2 kHz for standard rib spacing, when the vibratory wavelength is less than twice the mean distance between consecutive ribs. A simple formula is proposed in order to formally introduce a disorder parameter that accounts for the slight irregularity in rib spacing currently observed in piano soundboards. The statistics of the numerical and experimental rib distributions are discussed.

Above this frequency limit, modal shapes are hard to measure experimentally, and we must content ourselves with

measurements of ODS for a given excitation defined in space and frequency. Our calculations show that the ODS, viewed as the weighted sum of modal shapes where the weights depend on the location of the excitation, can also exhibit localization effects. These results are confirmed by a series of measured ODS for frequencies above 1.1 kHz. However, the generalization of these results is not proved yet, and remains an open question.

These phenomena have obvious consequences on string-soundboard coupling since the design of bridge and ribs affects the complete mobility pattern of the soundboard and, in particular, at the bridge. Another consequence of localization on radiation is that the directivity of the instrument is reduced, compared to idealized modes with regular pattern distributed all over the surface. The broadening of the directivity pattern due to real rib design, compared to the idealized fictitious case, was confirmed by computing radiation fields where the input is the spatial velocity distribution.

In this paper, all experiments were conducted on an upright piano. However, it can be reasonably anticipated that similar effects of rib distribution and bridge could be observed on a grand piano.

ACKNOWLEDGMENTS

The authors would like to thank Vincent Doutaut and Patrick Sinigaglia at ITEMM-Le Mans for enabling measurements on the Pleyel P131 soundboards.

[1]J. Harold and H. A. Conklin, "Design and tone in the mechanoacoustic piano. Part II. Piano structure," J. Acoust. Soc. Am. **100**, 695–708 (1996).
[2]P. H. Bilhuber and C. A. Johnson, "The influence of the soundboard on piano tone quality," J. Acoust. Soc. Am. **11**, 311–320 (1940).
[3]K. Wogram, "Acoustical research on pianos: vibrational characteristics of the soundboard," Das Musikinstrument **24**, 694–702, 776–782,872–880 (1980).
[4]U. Müller, "Influence of ribs on the acoustic behavior of piano resonant plates," Arch. Acoust. **5**, 147–155 (1980).
[5]H. Suzuki, "Vibration and sound radiation of a piano soundboard," J. Acoust. Soc. Am. **80**, 1573–1582 (1986).
[6]N. Giordano, "Simple model of a piano soundboard," J. Acoust. Soc. Am. **102**, 1159–1168 (1997).
[7]N. Giordano, "Mechanical impedance of a piano soundboard," J. Acoust. Soc. Am. **103**, 2128–2133 (1998).
[8]K. Ege and X. Boutillon, "Vibrational and acoustical characteristics of the piano soundboard," in *Proceedings of the 20th International Congress on Acoustics*, Sydney (2010), Paper No. 427.
[9]K. Ege and X. Boutillon, "Synthetic description of the piano soundboard mechanical mobility," in *Proceedings of the International Symposium on Musical Acoustics*, Sydney and Katoomba (2010), Paper No. 5.
[10]H. A. Conklin, "Soundboard construction for stringed musical instruments," U.S. patent 3866506 (February 18, 1975).
[11]P. Anderson, "Absence of diffusion in certain random lattices," Phys. Rev. **109**, 1492–1505 (1958).
[12]C. Pierre, "Mode localization and eigenvalue loci veering phenomena in disordered structures," J. Sound Vib. **126**, 485–502 (1988).
[13]C. Pierre, "Weak and strong vibration localization in disordered structures: A statistical investigation," J. Sound Vib. **139**, 111–132 (1990).
[14]Z. Chen and W. Xie, "Vibration localization in plates rib-stiffened in two orthogonal directions," J. Sound Vib. **280**, 235–262 (2005).
[15]See http://www-cast3m.cea.fr (Last viewed 11/20/2012).
[16]R. Hearmon, "The elasticity of wood and plywood," Forest Products Research Special Report No. 7, Her Majesty's Stationery Office, London (1948), pp. 1–87.
[17]V. Bucur, "Acoustics of Wood," in *Springer Series in Wood Science*, 2nd ed. (Springer, Heidelberg, 2006), Chap. 7.
[18]A. Papoulis and S. U. Pillai, *Probability, Random Variables and Stochastic Processes*, 4th ed. (McGraw-Hill, New York, 2002), Chap. 4–5, pp. 72–168.
[19]J. Berthaut, M. Ichchou, and L. Jézéquel, "Piano soundboard: Structural behavior, numerical and experimental study in the modal range," Appl. Acoust. **64**, 1113–1136 (2003).
[20]M. N. Ichchou, J. Berthaut, and M. Collet, "Multi-mode wave propagation in ribbed plates. Part II: Predictions and comparisons," Int. J. Solids Struct. **45**, 1196–1216 (2008).
[21]S. Yoshikawa, "Acoustical classification of woods for string instruments," J. Acoust. Soc. Am. **122**, 568–573 (2007).
[22]T. R. Moore and S. A. Zietlow, "Interferometric studies of a piano soundboard," J. Acoust. Soc. Am. **119**, 1783–1793 (2006).
[23]A. Mamou-Mani, J. Frelat, and C. Besnainou, "Numerical simulation of a piano soundboard under downbearing," J. Acoust. Soc. Am. **123**, 2401–2406 (2008).
[24]N. Atalla, J. Nicolas, and C. Gauthier, "Acoustic radiation of an unbaffled vibrating plate with general elastic boundary conditions," J. Acoust. Soc. Am. **99**, 1484–1494 (1996).